

# Microscopic derivation of pion-nucleon and pion-Delta scattering lengths

P. Bicudo<sup>1</sup>, M. Faria, G. M. Marques<sup>2</sup> and J. E. Ribeiro<sup>3</sup>

*Centro de Física das Interações Fundamentais (CFIF),  
Departamento de Física, Instituto Superior Técnico,  
Av. Rovisco Pais, 1049-001 Lisboa, Portugal*

---

## Abstract

A general expression for the  $\pi - N$  and  $\pi - \Delta$  scattering lengths is derived in the framework of a microscopic calculation. Annihilation, negative energy wavefunctions and spontaneous chiral symmetry are included consistently. The point-like limit is used to calculate the scattering lengths.

*Key words:*

preprint FISIST/18-2002/CFIF

PACS: 11.30.Rd, 12.39.Jh, 13.75.Gx

---

## 1 Introduction

In the last decade a global picture for low energy hadronic physics has slowly emerged. Although the theory of hadronic reactions, which one expects to be a consequence of QCD, remains as challenging as ever, we possess a natural symmetry (chiral symmetry) which acts, so to speak, as a filter for the still largely unknown low energy details of strong interactions. Indeed it is remarkable that although intermediate theoretical concepts like gluon propagators, quark effective masses and so on, might vary (in fact they are not gauge invariant and hence they are not physical observables), chiral symmetry contrives for the final physical results, e.g. hadronic masses and scattering lengths, to be largely insensitive to the above mentioned theoretical uncertainties. The pion mass furnishes the ultimate example. For massless quarks, the pion mass is

---

<sup>1</sup> bicudo@ist.utl.pt

<sup>2</sup> gmarques@cfif.ist.utl.pt

<sup>3</sup> emilio@netcabo.pt

bound to be zero, regardless of the form of the effective quark interaction *provided* it supports the mechanism of spontaneous breakdown of chiral symmetry ( $S\chi SB$ ).

$\pi - \pi$  elastic scattering [1,2,3,4] provides another example of this insensitivity to the form of the quark microscopic interaction. The incorporation of chiral symmetry in quark models has, in the history of hadronic physics, a long standing, starting with the attempts at restoring chiral symmetry to the MIT bag model [5,6,7,8]. Those models can be considered as realizations of a more general class of microscopic models, known as extended Nambu–Jonas-Lasinio [9] models (eNJL) [10,11,12,13,14,15], which in turn could be formally deduced from QCD through cumulant expansion [16] if we were to know all the gluon correlators. However, for practical applications, the set of all gluon correlators gets reduced to the Gaussian approximation (two gluon correlators). It simply turns out that chiral symmetry alleviates us from the burden of knowing in detail even this correlator. In fact,  $S\chi SB$  forces the quark-quark, quark-antiquark, antiquark-antiquark potentials together with the annihilation and creation interactions to originate from the *same* single chiral invariant Bethe-Salpeter kernel. Then it turns out, in what concerns  $\pi$ -hadron scattering lengths, that even this dependence is not *explicit* so that such scattering lengths are purely given in terms of hadronic masses and normalizations. Of course the implicit dependence on a given kernel is ensured by the actual values of those masses and normalizations for that kernel. But what is important to stress is that the formulae for the scattering lengths will not explicitly depend on such kernels and will therefore remain formally invariant for arbitrary kernels. The initial studies within eNJL models were aimed at studying the interplay between confinement and dynamical chiral symmetry breaking ( $D\chi SB$ ), and concentrated on critical couplings [10] for  $D\chi SB$  and light-meson spectroscopy [11]. Those NJL like models have been extended to study the pion beyond BCS level and meson resonant decays in the context of a generalized [14,17,18,19,20,21] resonating group method (RGM) [22].

In this paper we will derive the scattering lengths for the  $\pi - B$  system, with  $B$  standing for either  $N$  or  $\Delta$ . This notation will be used throughout this paper. The effects of quark-antiquark annihilation, of the relativistic negative energy component of the pion, and of the hadron exchange interaction will be consistently computed in the framework of the  $S\chi SB$ . This will also improve the state of the art [23,24] of the RGM.

This paper is organized as follows: in Section 2 we present the Hamiltonian and some useful definitions; in Section 3 we determine the RGM diagrams which contribute for the contact effective pion-hadron potential; Section 4 is devoted to the study of the Salpeter amplitudes of mesons and baryons; in Section 5 we compute the various contributions to  $\mathcal{O}_{\pi-B}^{\text{RGM}}$  and explain how to assemble them together; the computation of the one hadron exchange effective

potential can be avoided in the point-like limit; in Section 6 the full effective potential is computed just with the contact term; we conclude in Section 7. The technical details involving flavor and spin traces are left for Appendix A.

## 2 The Hamiltonian

The eNJL class of models correspond to the Gaussian approximation of QCD in the cumulant expansion in terms of gluon correlators,

$$H = \int d^3x q^\dagger(x)(-i\boldsymbol{\alpha} \cdot \boldsymbol{\nabla} + m\beta)q(x) - \frac{i}{2} \int d^3x \int d^3y \bar{q}(x)\gamma^\mu T^a q(x)\bar{q}(y)\gamma^\nu T^b q(y)\langle\langle gA_\mu^a(x)gA_\nu^b(y)\rangle\rangle, \quad (1)$$

The Gaussian correlator  $\langle\langle gA_\mu^a(x)gA_\nu^b(y)\rangle\rangle$  turns out to be identical to the vacuum expectation of  $K(x, y) = \langle gA_\mu^a(x)gA_\nu^b(y)\rangle$ . Translation invariance,  $K(x, y) = K(x - y)$  is assumed throughout this paper. In Eq. (1) the  $T^a$  stands for the Gell-Mann generator  $\lambda^a/2$  and the quark field  $q(\boldsymbol{x})$  is given by

$$q(\boldsymbol{x}) = \sum_s \int \frac{d^3k}{(2\pi)^3} [u_s(\mathbf{k})b_{\mathbf{k}s} + v_s(\mathbf{k})d_{-\mathbf{k}s}^\dagger] e^{i\mathbf{k}\cdot\mathbf{x}}, \quad (2)$$

with

$$\begin{aligned} u_s(\mathbf{k}) &= \left[ \sqrt{\frac{1+S(k)}{2}} + \sqrt{\frac{1-S(k)}{2}} \hat{\mathbf{k}} \cdot \boldsymbol{\alpha} \right] u_s(0), \\ v_s(\mathbf{k}) &= \left[ \sqrt{\frac{1+S(k)}{2}} - \sqrt{\frac{1-S(k)}{2}} \hat{\mathbf{k}} \cdot \boldsymbol{\alpha} \right] v_s(0). \end{aligned} \quad (3)$$

For the quark spinors  $u_\uparrow(\mathbf{0}) = (1, 0, 0, 0)$ ,  $u_\downarrow(\mathbf{0}) = (0, 1, 0, 0)$ ,  $v_\uparrow(\mathbf{0}) = (0, 0, 0, 1)$  and  $v_\downarrow(\mathbf{0}) = (0, 0, -1, 0)$ . In Eq. (3)  $S(k)$  is a shorthand notation for  $\sin \phi(k)$  the solution of the S $\chi$ SB mass gap equation. For details on the solution of the mass gap equation see Ref. [10,12,13,25]. Following this reference we arrive at the set of possible quark-quark, quark-antiquark and antiquark-antiquark vertices, which are defined in Table 1, with the convention of representing the quark with a single line and the antiquark with a double line. For completeness we also represent in the last entry the single-quark (antiquark) energy  $E(p)$ , as a function of the modulus of the momentum  $\mathbf{p}$ .

The set of all diagrams which can be built from the basic vertices of Table 1 fall into two disjoint classes:

Table 1

The microscopic vertices for the coupling of the potential rung with the quark and antiquark lines.

Quark vertex	$\Gamma^{qq}$	$u_s^\dagger(k)\beta\gamma^\mu u_{s'}(k')$	
Antiquark vertex	$\Gamma^{\bar{q}\bar{q}}$	$-v_s^\dagger(k)\beta\gamma^\mu v_{s'}(k')$	
Creation vertex	$\Gamma^{q\bar{q}}$	$u_s^\dagger(k)\beta\gamma^\mu v_{s'}(k')$	
Annihilation vertex	$\Gamma^{\bar{q}q}$	$v_s^\dagger(k)\beta\gamma^\mu u_{s'}(k')$	
Kinetic energy	$T_p$		

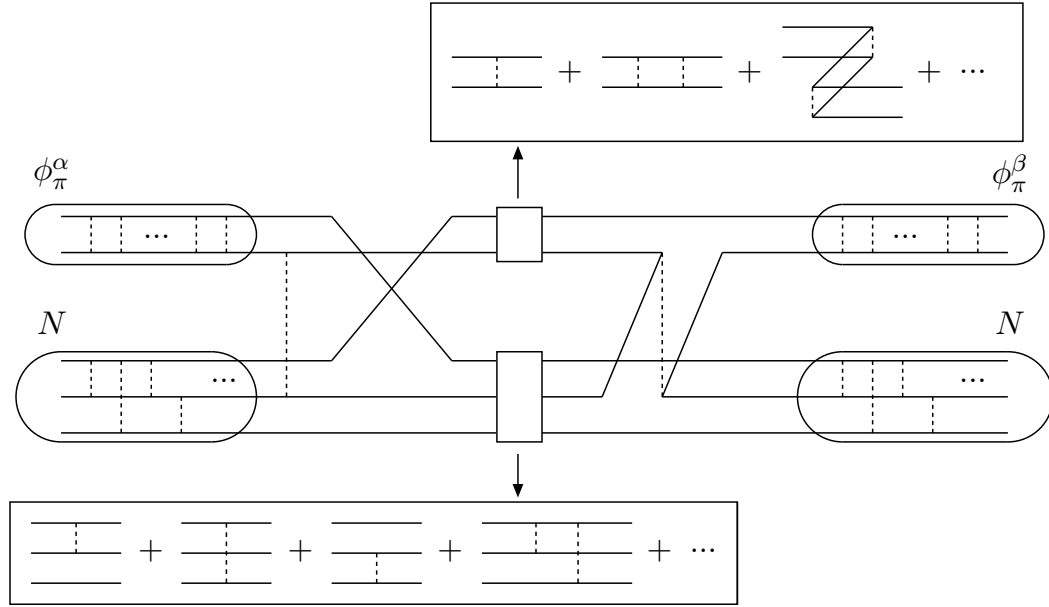


Fig. 1. Example of a diagram with intermediate hadrons

- Diagrams in which no intermediate hadron propagator can be cut. As an example of diagrams belonging to this class see Fig. 2. We call the diagrams belonging to this class contact diagrams.
- The complementary class of diagrams having an intermediate hadron. See Fig. 1 for an example.

In the remainder of his paper we will derive the  $\pi$ -Baryon ( $\pi - B$ ) scattering lengths,  $a_{\pi-B}$ .

### 3 The Resonating Group Method evaluation of $a_{\pi-B}$

To compute the  $T_{\pi-B}$  transition matrix we follow the RGM to obtain the effective  $\pi - B$  potential  $\mathcal{O}_{\pi-B}^{\text{RGM}}$ . To see how to derive the RGM formalism for eNJL Hamiltonians see ref. [14,17,18,19,20,21], where it was shown that the

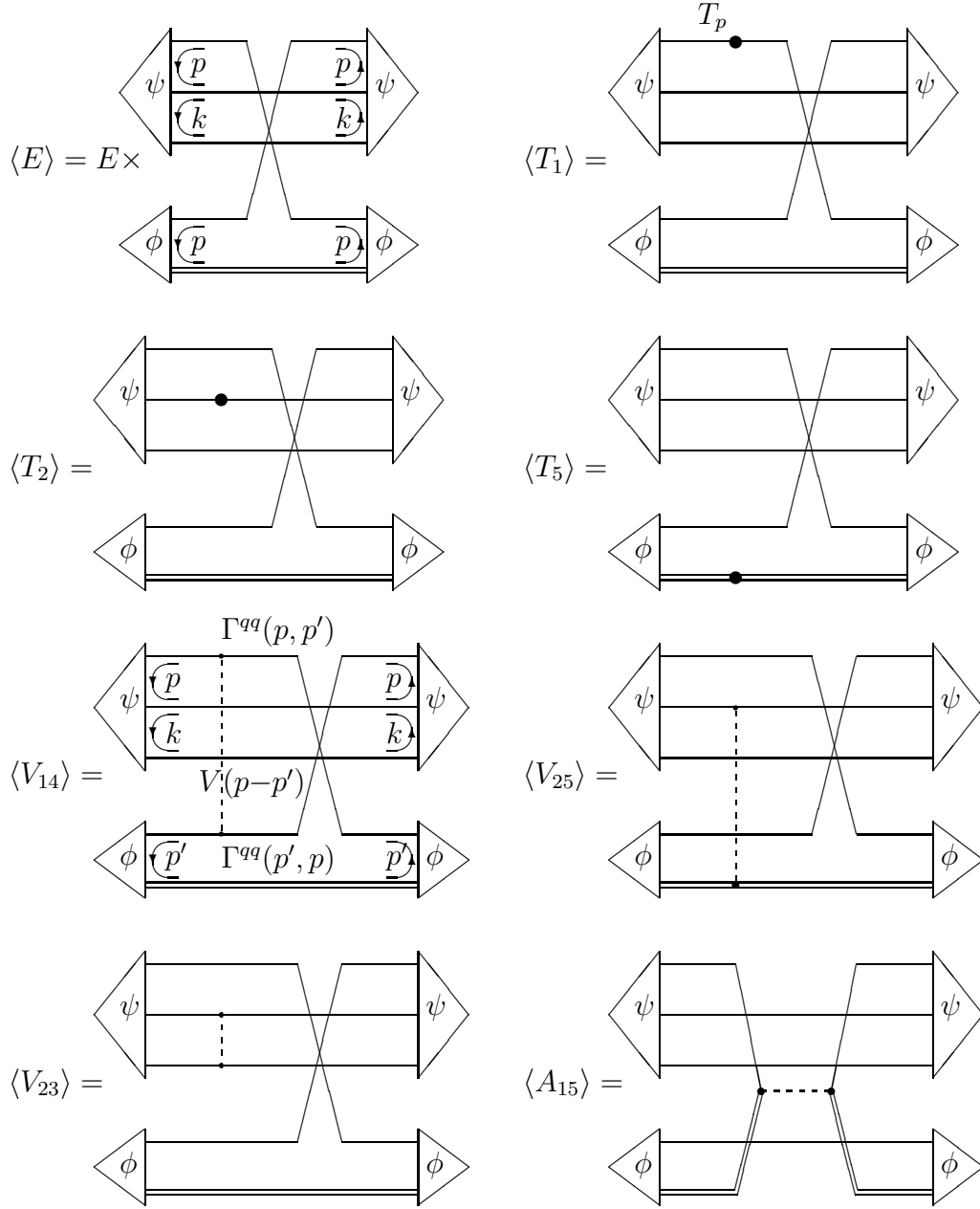


Fig. 2. Energy, kinetic and potential overlaps contributing to meson-hadron scattering. The dot corresponds to the insertion of a kinetic operator.

RGM equations for hadronic scattering, being dynamical equations for coupled channels of boundstates and resonances scattering, are simply obtained by replacing in the S matrix Dyson equations the correspondent solutions of the Bethe-Salpeter equations for each of the intervening hadrons. We get

$$\mathcal{O}_{\pi-B}^{\text{RGM}} = \langle 3E - 6T_1 - 6T_2 - 3T_5 - 3V_{23} + 3V_{14} + 6V_{25} + 3A_{15} \rangle, \quad (4)$$

where the factors 3 and 6 are there to account for all the possible permutations in the exchange of quarks and the minus signs are produced by the Pauli

principle. The existence of negative energy spin amplitudes for the mesons complicates considerably the RGM calculations. In order to take into account this degree of freedom we will proceed in two steps. First we will only consider those diagrams containing positive energy amplitudes and later we extend this set of diagrams to those containing the negative energy amplitudes. For the moment let us consider only the positive energy amplitudes.

The different terms of Eq. (4) are represented by the diagrams in Fig. 2. For instance diagrams  $\langle E \rangle$  and  $\langle V_{14} \rangle$  correspond to the integrals

$$\langle E \rangle = \sum_{s_i} \int \frac{d^3 p}{(2\pi)^3} \frac{d^3 k}{(2\pi)^3} \Psi_{s_1, s_2, s_3}^\dagger(\mathbf{p}, \mathbf{k}) \Psi_{s_4, s_2, s_3}(\mathbf{p}, \mathbf{k}) \phi_{s_1, s_5}^\dagger(\mathbf{p}) \phi_{s_4, s_5}(\mathbf{p}) \quad (5)$$

$$\langle V_{14} \rangle = \sum_{s_i} \int \frac{d^3 p}{(2\pi)^3} \frac{d^3 p'}{(2\pi)^3} \frac{d^3 k}{(2\pi)^3} \Psi_{s_1, s_2, s_3}^\dagger(\mathbf{p}, \mathbf{k}) \Psi_{s_7, s_2, s_3}(\mathbf{p}, \mathbf{k}) \Gamma_{s_1, s_6}^{qq}(\mathbf{p}, \mathbf{p}') V(\mathbf{p} - \mathbf{p}') \Gamma_{s_4, s_7}^{qq}(\mathbf{p}', \mathbf{p}) \phi_{s_4, s_5}^\dagger(\mathbf{p}') \phi_{s_6, s_5}(\mathbf{p}') , \quad (6)$$

where  $V(\mathbf{p} - \mathbf{p}')$  represents the Fourier transform of a generic quark kernel  $K(x - y)$  which we do not need to know. In Eq. (6)  $\phi$  and  $\Psi$  are the Salpeter amplitudes for pions and baryons respectively.

Fig. 2 includes all topologically possible diagrams, except for diagrams which interaction can be included from the onset in the energy of the external bound states. All diagrams, except for  $\langle A_{15} \rangle$ , include a quark exchange because a simple kernel insertion (which goes with  $\frac{\bar{\lambda}}{2} \cdot \frac{\bar{\lambda}}{2}$  in color space) has zero matrix element between color singlets.

The diagrams  $\langle V_{14} \rangle$  and  $\langle V_{25} \rangle$  are the usual RGM diagrams yielding for most reactions a repulsive force. This is the case of Nucleon-Nucleon elastic scattering where they are shown to provide a substantial repulsion [22,26]. The same happens with exotic meson-meson reactions. Retrospectively we can say that the success of the present calculation constitutes an extension of these results.

The diagram  $\langle A_{15} \rangle$  contains quark-antiquark annihilation amplitudes and for most cases it provides for attraction [27].

Then  $a_{\pi-B}$  is given by

$$a_{\pi-B} = -\mu_{red} \mathcal{O}_{\pi-B}^{\text{RGM}} / (2\pi + 2\mu_{red} \mathcal{O}_{\pi-B}^{\text{RGM}} N^{2/3}). \quad (7)$$

In Eq. (7)  $\mu_{red}$  is the reduced mass of the system  $\pi - B$ ,

$$\mu_{red} = M_\pi - M_\pi^2 / M_B + \dots , \quad (8)$$

and the simple Born approximation already provides the leading order in  $M_\pi$

$$a_{\pi-B} = -M_\pi \mathcal{O}_{\pi-B}^{\text{RGM}} / (2\pi) . \quad (9)$$

$$\begin{aligned}
[E - 2T_p] \times \begin{array}{c} \text{---} \\ \text{---} \\ \text{---} \end{array} \begin{array}{c} \text{---} \\ \text{---} \\ \text{---} \end{array} \phi^+ &= \begin{array}{c} \Gamma^{qq}(p, p') \\ \text{---} \\ V(p-p') \\ \text{---} \\ \Gamma^{\bar{q}\bar{q}}(p, p') \end{array} \begin{array}{c} \text{---} \\ \text{---} \\ \text{---} \end{array} \phi^+ + \begin{array}{c} \text{---} \\ \text{---} \\ \text{---} \end{array} \begin{array}{c} \text{---} \\ \text{---} \\ \text{---} \end{array} \phi^- \\
[-E - 2T_p] \times \begin{array}{c} \text{---} \\ \text{---} \\ \text{---} \end{array} \phi^- &= \begin{array}{c} \Gamma^{\bar{q}q} \\ \text{---} \\ V \\ \text{---} \\ \Gamma^{\bar{q}q} \end{array} \begin{array}{c} \text{---} \\ \text{---} \\ \text{---} \end{array} \phi^+ + \begin{array}{c} \text{---} \\ \text{---} \\ \text{---} \end{array} \begin{array}{c} \text{---} \\ \text{---} \\ \text{---} \end{array} \phi^-
\end{aligned}$$

Fig. 3. Salpeter coupled equations for a quark and an antiquark in a meson. In most mesons the negative energy component  $\phi^-$  is negligible which simplifies the equation to a single Schrödinger equation

In order to calculate  $\mathcal{O}_{\pi-B}^{\text{RGM}}$  we need first to know the Salpeter solutions for the asymptotic pions and baryons which will then act as wave-functions for the ordinary RGM equations. As we have already stated this recipe is equivalent to solve the complete Dyson series for  $\pi - B$  scattering for contact diagrams. For a detailed proof of this equivalence see ref. [14,17,18,19,20,21].

#### 4 Salpeter equations for mesons and baryons

In this section we give the Salpeter amplitudes for mesons and  $B$ s. Since we are considering s-wave hadrons the angular momentum is trivial, and the spin is expected to dominate dynamics. The independent spin degrees of freedom correspond to a spin singlet and a spin triplet. For instance, in the  $\Delta$  the diquarks are in a spin triplet state whereas in the  $N$  they have a mixed spin structure  $(F_{\text{spin}} F_{\text{flavor}} + D_{\text{spin}} D_{\text{flavor}})/\sqrt{2}$ , where the  $F$  component is a singlet and the  $D$  component a triplet. In the meson sector the spin structure is clearer. The  $\pi$  meson is a spin singlet and the  $\rho$  meson is a spin triplet. Besides spin structure we have another degree of freedom known as the energy-spin which takes into account the positive and negative energy Salpeter amplitudes. These negative energy amplitudes play a major role in the Goldstone nature of the pion, being much less relevant for the  $\rho$  case. In the present work these mesonic negative energy amplitudes will be fully taken into account. There are no negative energy amplitudes for the  $B$ s [28].

The bound state equations for hadrons are essentially quark-antiquark Salpeter or RPA equation in the case of mesons, see Fig. 3, and Schrödinger or TDA equation for three quarks case of baryons, see Fig. 4. In Fig. 3 the mesonic Salpeter equation consists in fact of two coupled equations, coupling posi-

Fig. 4. Schrödinger equation for 3 quarks in a baryon

tive to negative energy amplitudes. As an example, we can use the vertices definitions of Table 1 to write one of these equations (the topmost) as

$$\begin{aligned}
H\phi_{s_1,s_2}^+(p) &= [T_p + T_{-p}]\phi_{s_1,s_2}^+(p) + \\
&+ \sum_{s_3,s_4} \int \frac{d^3p'}{(2\pi)^3} \Gamma_{s_1,s_3}^{qq}(\mathbf{p}, \mathbf{p}') V(\mathbf{p} - \mathbf{p}') \Gamma_{s_2,s_4}^{\bar{q}\bar{q}}(\mathbf{p}', \mathbf{p}) \phi_{s_3,s_4}^+(p') + \\
&+ \sum_{s_3,s_4} \int \frac{d^3p'}{(2\pi)^3} \Gamma_{s_1,s_3}^{q\bar{q}}(\mathbf{p}, \mathbf{p}') V(\mathbf{p} - \mathbf{p}') \Gamma_{s_2,s_4}^{\bar{q}q}(\mathbf{p}', \mathbf{p}) \phi_{s_3,s_4}^-(p') \\
&= E\phi_{s_1,s_2}^+(p) .
\end{aligned} \tag{10}$$

In particular Eq. (10) reduces to the Schrödinger equation for mesons when the coupling to the negative energy  $\phi^-$  wave-function is negligible.

The next step consists in working out the spin $\times$ flavour $\times$ colour traces. These traces are worked out in appendix A. Doing this will lead us, in the case of mesons, to the following two coupled channel equations,

$$H_m(\mathbf{p}) \begin{bmatrix} |\phi_m^+\rangle \\ |\phi_m^-\rangle \end{bmatrix} = \int \frac{d^3q}{(2\pi)^3} \mathcal{H}(\mathbf{p}, \mathbf{q}) \begin{bmatrix} |\phi_m^+\rangle \\ |\phi_m^-\rangle \end{bmatrix} = M_m \sigma^3 \begin{bmatrix} |\phi_m^+\rangle \\ |\phi_m^-\rangle \end{bmatrix}, \tag{11}$$

with

$$\mathcal{H}(\mathbf{p}, \mathbf{q}) = \begin{bmatrix} 2T_p \delta(\mathbf{p} - \mathbf{q}) + V_m^{++}(\mathbf{p}, \mathbf{q}) & V_m^{+-}(\mathbf{p}, \mathbf{q}) \\ V_m^{-+}(\mathbf{p}, \mathbf{q}) & 2T_p \delta(\mathbf{p} - \mathbf{q}) + V_m^{--}(\mathbf{p}, \mathbf{q}) \end{bmatrix}, \tag{12}$$

where  $V_m^{++}$ ,  $V_m^{+-}$ ,  $V_m^{-+}$  and  $V_m^{--}$  contain the aforementioned spin traces.

#### 4.1 The pion case

First we work out the spin traces for the pion case. We have,

$$\begin{aligned}
V_{\pi}^{++}(\mathbf{p}, \mathbf{p}') &= \frac{4}{3} Tr\{\Sigma^{\pi} \cdot \Gamma_{p,p'}^{\bar{q}q} \cdot \Sigma^{\pi\dagger} \cdot \Gamma_{p',p}^{qq}\} V(\mathbf{p} - \mathbf{p}') \\
&= -\frac{2}{3} Tr\{\Gamma_{p,p'}^{qq} \Gamma_{p',p}^{qq}\} V(\mathbf{p} - \mathbf{p}') , \\
V_{\pi}^{+-}(\mathbf{p}, \mathbf{p}') &= \frac{4}{3} Tr\{\Sigma^{\pi} \cdot \Gamma_{p,p'}^{\bar{q}q} \cdot \Sigma^{\pi} \cdot \Gamma_{p',p}^{\bar{q}q}\} V(\mathbf{p} - \mathbf{p}') \\
&= -\frac{2}{3} Tr\{\Gamma_{p,p'}^{\bar{q}q} \Gamma_{p',p}^{\bar{q}q}\} V(\mathbf{p} - \mathbf{p}') .
\end{aligned} \tag{13}$$

where  $\Sigma^{\pi}$  stands for the pion spin wave function defined in Appendix A along with spin wave functions for other relevant hadrons. Notice that  $V_{\pi}^{+-}$  acts as a potential coupling the negative energy wave-function  $\phi^{-}$  with the positive energy wave-function  $\phi^{+}$ .  $V_{\pi}^{++}$  stands as the usual potential binding the quark and the antiquark in the positive energy wave-function  $\phi^{+}$ . The color factor  $4/3$  is included in the  $V$ 's definition for simplicity. The relations

$$\Gamma^{qq} = (i\sigma_2)\Gamma^{\bar{q}q}(i\sigma_2) , \quad \Gamma^{q\bar{q}} = -(i\sigma_2)\Gamma^{\bar{q}q}(i\sigma_2) , \tag{14}$$

were used. They hold for both the Dirac vertices  $\gamma^0$  and  $\vec{\gamma}$ .

The pion occupies a singular position, insofar it is the only bound state where  $\phi_{\pi}^{-}$  is not negligible. In particular  $|\phi_{\pi}^{-}|$  is just slightly smaller than  $|\phi_{\pi}^{+}|$  because the  $\pi$  is nearly a Goldstone boson. The Salpeter pion wave functions are

$$\phi^{\pm}(\mathbf{k}) = \frac{S(\mathbf{k})}{a} \pm a \xi(\mathbf{k}) \quad \text{with} \quad a = \sqrt{\frac{2M_{\pi}}{3}} f_{\pi} , \tag{15}$$

where  $f_{\pi}$  is the well known pion decay constant,  $S(k)$  determines the extent of dynamical chiral symmetry breaking and  $\xi(k)$  is related to normalization of the wave function. The Salpeter wave functions are normalized as follows,

$$\begin{aligned}
\left[ \langle \phi^{+} | \langle \phi^{-} | \right] \sigma^3 \begin{bmatrix} | \phi^{+} \rangle \\ | \phi^{-} \rangle \end{bmatrix} &= \int \frac{d^3k}{(2\pi)^3} (\phi^{+}(\mathbf{k})^2 - \phi^{-}(\mathbf{k})^2) = \\
= 4 \int \frac{d^3k}{(2\pi)^3} S(\mathbf{k}) \xi(\mathbf{k}) &= \frac{2}{a} \int \frac{d^3k}{(2\pi)^3} S(\mathbf{k}) (\phi^{+}(\mathbf{k}) - \phi^{-}(\mathbf{k})) = 1 .
\end{aligned} \tag{16}$$

## 4.2 The rho case

For the  $\rho$  we can follow exactly the same steps as in the pion case to get

$$V_\rho^{++}(\mathbf{p}, \mathbf{p}') = -\frac{2}{9} Tr\{\sigma^k \Gamma_{p,p'}^{qq} \sigma^k \Gamma_{p',p}^{qq}\} \delta_{ss'} V(\mathbf{p} - \mathbf{p}') . \quad (17)$$

To obtain Eq. (17) the following identity

$$\int \frac{d^3 p}{(2\pi)^3} \frac{d^3 p'}{(2\pi)^3} Tr\{\sigma^i \Gamma_{p,p'}^{qq} \sigma^j \Gamma_{p',p}^{qq}\} = \int \frac{d^3 p}{(2\pi)^3} \frac{d^3 p'}{(2\pi)^3} \frac{1}{3} Tr\{\sigma^k \Gamma_{p,p'}^{qq} \sigma^k \Gamma_{p',p}^{qq}\} \delta^{ij} , \quad (18)$$

must be used.

The potential  $V_\rho^{+-}(\mathbf{p}, \mathbf{p}')$  can also be computed and it turns out that it is exactly equal to  $-1/3$  of  $V_\pi^{+-}(\mathbf{p}, \mathbf{p}')$ . It provides a negligible coupling of  $\phi_\rho^-$  to  $\phi_\rho^+$  and this is the technical reason why the  $\rho$  is essentially a Schrödinger bound state.

## 4.3 The baryon case

In the case of the baryons we have no negative energy amplitude (there is no way with a two body kernel of simultaneously reversing three quark lines) and we need only to consider the  $V_B^{++}$ . Following the same steps used in deriving Eqs. (13) and (17) we get,

$$\begin{aligned} V_{N^F}^{++}(\mathbf{p}, \mathbf{p}') &= 3 \frac{2}{3} Tr\{\Sigma_s^{N^F} \cdot \Gamma_{p-k, p'-k}^{qq} \cdot \Sigma_{s'}^{N^F \dagger} \cdot \Gamma_{p, p'}^{qq}\} V(\mathbf{p} - \mathbf{p}') \\ &= -2 \frac{1}{2} Tr\{\Gamma_{p'-k, p-k}^{qq} \Gamma_{p, p'}^{qq}\} \delta_{ss'} V(\mathbf{p} - \mathbf{p}') \\ &= -Tr\{\Gamma_{p'-k, p-k}^{qq} \Gamma_{p, p'}^{qq}\} \delta_{ss'} V(\mathbf{p} - \mathbf{p}'), \end{aligned} \quad (19)$$

$$\begin{aligned} V_{N^D}^{++}(\mathbf{p}, \mathbf{p}') &= 3 \frac{2}{3} Tr\{\Sigma_s^{N^D} \cdot \Gamma_{p-k, p'-k}^{qq} \cdot \Sigma_{s'}^{N^D \dagger} \cdot \Gamma_{p, p'}^{qq}\} V(\mathbf{p} - \mathbf{p}') \\ &= -2 \frac{1}{6} Tr\{\sigma^i \Gamma_{p'-k, p-k}^{qq} \sigma^j \Gamma_{p, p'}^{qq}\} \sigma_{sc}^i \sigma_{cs'}^j V(\mathbf{p} - \mathbf{p}') \\ &= -\frac{1}{3} Tr\{\sigma^k \Gamma_{p'-k, p-k}^{qq} \sigma^k \Gamma_{p, p'}^{qq}\} \delta_{ss'} V(\mathbf{p} - \mathbf{p}'), \end{aligned} \quad (20)$$

$$\begin{aligned}
V_{\Delta}^{++}(\mathbf{p}, \mathbf{p}') &= 3 \frac{2}{3} \text{Tr} \{ \Sigma_s^{\Delta} \cdot \Gamma_{p-k, p'-k}^{qq} \cdot \Sigma_{s'}^{\Delta \dagger} \cdot \Gamma_{p, p'}^{qq} \} V(\mathbf{p} - \mathbf{p}') \\
&= -3 \frac{1}{3} \text{Tr} \{ \sigma^i \Gamma_{p'-k, p-k}^{qq} \sigma^j \Gamma_{p, p'}^{qq} \} w_{sc}^i w_{cs'}^j V(\mathbf{p} - \mathbf{p}') \quad (21) \\
&= -\frac{1}{3} \text{Tr} \{ \sigma^k \Gamma_{p'-k, p-k}^{qq} \sigma^k \Gamma_{p, p'}^{qq} \} \delta_{ss'} V(\mathbf{p} - \mathbf{p}').
\end{aligned}$$

Along with the color factors we include the factor three that accounts for the number of diagrams. We checked numerically, for various microscopic kernels (like for example the  $r^2$  harmonic kernel) that, under integration in  $k$ ,  $V_{NF}^{++}$ ,  $V_{ND}^{++}$  and  $V_{\Delta}^{++}$  are, to a good approximation, given by,

$$\begin{aligned}
V_{NF}^{++}(\mathbf{p}, \mathbf{p}') &\simeq \frac{3}{2} V_{\pi}^{++}(\mathbf{p}, \mathbf{p}') \delta_{ss'}, \\
V_{ND}^{++}(\mathbf{p}, \mathbf{p}') &\simeq \frac{3}{2} V_{\rho}^{++}(\mathbf{p}, \mathbf{p}') \delta_{ss'}, \quad (22) \\
V_{\Delta}^{++}(\mathbf{p}, \mathbf{p}') &\simeq \frac{3}{2} V_{\rho}^{++}(\mathbf{p}, \mathbf{p}') \delta_{ss'},
\end{aligned}$$

For the various quark kernels, the errors for the  $N$  and  $\Delta$  masses when using Eqs. (22) instead of Eqs. (19), (20) and (21), were always below 7%.

Having the spin  $\times$  flavor nucleon structure in mind – see Appendix A – we get,

$$\begin{aligned}
V_N^{++} &= \frac{3}{4} (V_{\pi}^{++} + V_{\rho}^{++}) \delta_{ss'}, \\
V_{\Delta}^{++} &= \frac{3}{2} V_{\rho}^{++} \delta_{ss'}. \quad (23)
\end{aligned}$$

In this case the baryon Salpeter amplitude will depend only on the diquark inner momentum and the baryon Salpeter amplitude is given by,

$$\Psi(\mathbf{p}) \simeq S(p) / \mathcal{N} \quad (24)$$

where  $\mathcal{N}$  is the baryon wave function normalization which is essentially the same for both  $N$  and  $\Delta$ .

#### 4.4 Summary

The results of the previous subsections can be summarized as follows,

$$\begin{aligned}
H_\pi \begin{bmatrix} |\phi_\pi^+\rangle \\ |\phi_\pi^-\rangle \end{bmatrix} &= \int \frac{d^3q}{(2\pi)^3} \mathcal{H}_\pi(\mathbf{p}, \mathbf{q}) \begin{bmatrix} |\phi_\pi^+\rangle \\ |\phi_\pi^-\rangle \end{bmatrix} = M_\pi \sigma^3 \begin{bmatrix} |\phi_\pi^+\rangle \\ |\phi_\pi^-\rangle \end{bmatrix}; \\
H_\rho |\phi_\rho\rangle &= \int \frac{d^3q}{(2\pi)^3} \mathcal{H}_\rho(\mathbf{p}, \mathbf{q}) |\phi_\rho\rangle = M_\rho |\phi_\rho\rangle; \\
\mathcal{H}_\rho(\mathbf{p}, \mathbf{q}) &= [2T_p \delta(\mathbf{p} - \mathbf{q}) + V_\rho^{++}(\mathbf{p}, \mathbf{q})]; \\
H_N |\Psi_N\rangle &= \int \frac{d^3q}{(2\pi)^3} \mathcal{H}_N(\mathbf{p}, \mathbf{q}) |\Psi_N\rangle = M_N |\Psi_N\rangle; \\
\mathcal{H}_N(\mathbf{p}, \mathbf{q}) &= \frac{3}{2} \left[ 2T_p \delta(\mathbf{p} - \mathbf{q}) + \frac{V_\pi^{++}(\mathbf{p}, \mathbf{q}) + V_\rho^{++}(\mathbf{p}, \mathbf{q})}{2} \right]; \\
H_\Delta |\Psi_\Delta\rangle &= \int \frac{d^3q}{(2\pi)^3} \mathcal{H}_\Delta(\mathbf{p}, \mathbf{q}) |\Psi_\Delta\rangle = M_\Delta |\Psi_\Delta\rangle; \\
\mathcal{H}_\Delta(\mathbf{p}, \mathbf{q}) &= \frac{3}{2} [2T_p \delta(\mathbf{p} - \mathbf{q}) + V_\rho^{++}(\mathbf{p}, \mathbf{q})] .
\end{aligned} \tag{25}$$

Eq. (25) predicts that  $M_\Delta = (3/2)M_\rho$ . This is a natural relation in the quark model and it is experimentally correct within 7% discrepancy. This suggests that neglecting both the negative energy wave-function  $\phi_\rho^-$  and the diquark recoil in the baryons are not unreasonable approximations for low energy scattering (scattering lengths).

### 5 Assembling the $\pi - B$ RGM overlaps $\mathcal{O}_{\pi-B}^{\text{RGM}}$

Before computing the flavor contribution to the RGM overlaps of Fig. 2, we have to extend the class of diagrams in Fig. 2 including the diagrams that couple to the negative energy wave function  $\phi_\pi^-$  of the external pions. The negative energy wave function is defined in Fig. 3 and in Eqs. (10) and (15).

For simplicity the negative energy wave function  $\phi_\pi^-$  was not included in the set of diagrams of Fig. 2. As we said, only  $\phi_\pi^+$  were included. There an incoming meson is a Dirac bra that couples to the right side of the RGM diagrams and an outgoing meson is a Dirac ket that couples to the left side of the RGM diagrams. To obtain the full set of the RGM overlaps, containing both  $\phi_\pi^+$  and  $\phi_\pi^-$  it is sufficient to notice that negative energy wave functions  $\phi_\pi^-$  must couple as Dirac bras to the right side of the diagram when they are outgoing and as Dirac kets to the left side when they are incoming and that they can only come in pairs either of two  $\phi_\pi^+$ s or two  $\phi_\pi^-$ s. The only possible topologies are

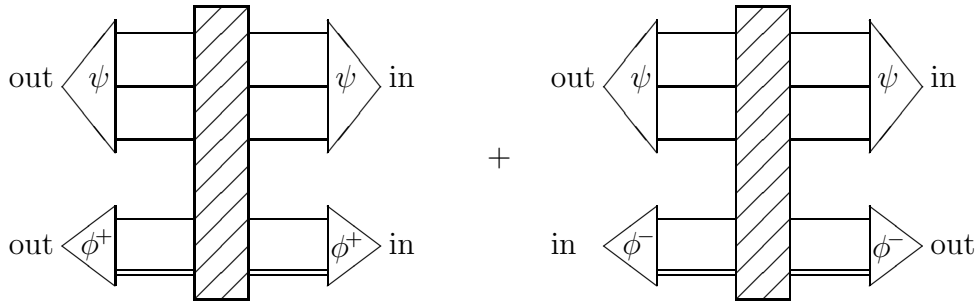


Fig. 5. Including the negative energy wave functions  $\phi_{\pi}^{-}$  in the RGM overlaps.

depicted in Fig. 5. Including  $\phi_{\pi}^{-}$ s amounts to double the number of diagrams of Fig.2. This has been studied in detail in Refs. [2,14,18].

In general  $\langle \mathcal{O}_{\pi-B}^{\text{RGM}} \rangle = \langle \mathcal{O}_{\pi-B}^{\text{RGM}} \rangle_{\text{colour}} \langle \mathcal{O}_{\pi-B}^{\text{RGM}} \rangle_{\text{spin} \times \text{flavour} \times \text{momentum}}$ . Therefore we need to disentangle the various contributions for  $\mathcal{O}_{\pi-B}^{\text{RGM}}$  in the spin  $\times$  flavour  $\times$  momentum space. To achieve this it is enough to notice two things: 1 - In the case of the nucleon,  $B = N$ , the spin gets mixed with flavour due to the fact that the spin  $\times$  flavour nucleon wave function is given by  $(F_{\text{spin}} F_{\text{flavour}} + D_{\text{spin}} D_{\text{flavour}})/\sqrt{2}$ . There is no such mixing in the case of the  $\Delta$ . Therefore in order to disentangle the spin  $\times$  flavour is enough to work separately for the F and D spin components. 2 - The flavour gets mixed with momentum due to the presence of negative energy amplitudes. This is a curious effect deserving some explanation. From the discussion in the introduction of this section we can have either two  $\phi^{+}$ s or two  $\phi^{-}$ s. When going from  $\phi^{+}$  to  $\phi^{-}$  what was a ket state becomes a bra state and vice versa. That is, the position of the two  $\phi$ s in the trace get interchanged when we go from  $\phi^{+}$  to  $\phi^{-}$ . In general this is enough to make the flavour traces to distinguish between the two cases. The same effect would have occurred in the spin case would it not be for the fact the pion has no total spin. Again, in order to disentangle flavour  $\times$  momentum it is enough to give the flavour results discriminated in  $\phi^{+}\phi^{+}$  and  $\phi^{-}\phi^{-}$ .

Having the above considerations in mind we now proceed to the separate evaluation of colour, spin, flavour and momentum contributions to  $\mathcal{O}_{\pi-B}^{\text{RGM}}$ .

### 5.1 Spin and colour contributions to $\mathcal{O}_{\pi-B}^{\text{RGM}}$

The spin and colour contributions to RGM are independent of the energy-spin degree of freedom and therefore can be evaluated for the diagrams of Fig. 2. The colour contributions to  $\mathcal{O}_{\pi-B}^{\text{RGM}}$  are given in Table 2. As for the spin, we give in Table 3 the results for  $\mathcal{O}_{\pi-B}^{\text{RGM}}$  discriminated by F and D spin components for the nucleon case. Notice that this overlaps are given in terms of the Salpeter  $V_{\pi}^{++}$ ,  $V_{\pi}^{+-}$ ,  $V_{\rho}^{++}$ ,  $V_{N_F}$ ,  $V_{N_D}$  and  $V_{\Delta}$  discussed in Section 4. For instance, the annihilation overlap  $\langle A_{15} \rangle$  is proportional to the  $V_{\pi}^{+-}$  that couples

Table 2

Color contributions.

$\langle E \rangle, \langle T_i \rangle$	$\langle V_{14} \rangle$	$\langle V_{25} \rangle$	$\langle V_{23} \rangle$	$\langle A_{15} \rangle$
$\frac{1}{3}$	$\frac{4}{9}$	$-\frac{2}{9}$	$-\frac{2}{9}$	$\frac{4}{9}$

Table 3

Spin contributions

	$N\pi$		$\Delta\pi$
	F	D	
$\langle E \rangle, \langle T_i \rangle$	$\frac{1}{2}\delta_{ss'}$	$\frac{1}{2}\delta_{ss'}$	$\frac{1}{2}\delta_{ss'}$
$\langle V_{14} \rangle$	$-\frac{3}{8}V_{\pi^{++}}(\mathbf{p}, \mathbf{q})\delta_{ss'}$	$-\frac{3}{8}V_{\pi^{++}}(\mathbf{p}, \mathbf{q})\delta_{ss'}$	$-\frac{3}{8}V_{\pi^{++}}(\mathbf{p}, \mathbf{q})\delta_{ss'}$
$\langle V_{25} \rangle$	$-\frac{1}{4}V_{N^F}(\mathbf{p}, \mathbf{q})$	$-\frac{1}{4}V_{N^D}(\mathbf{p}, \mathbf{q})$	$-\frac{1}{4}V_{\Delta}(\mathbf{p}, \mathbf{q})$
$\langle V_{23} \rangle$	$\frac{1}{4}V_{N^F}(\mathbf{p}, \mathbf{q})$	$\frac{1}{4}V_{N^D}(\mathbf{p}, \mathbf{q})$	$\frac{1}{4}V_{\Delta}(\mathbf{p}, \mathbf{q})$
$\langle A_{15} \rangle$	$-\frac{3}{8}V_{\pi^{+-}}(\mathbf{p}, \mathbf{q})\delta_{ss'}$	$-\frac{3}{8}V_{\pi^{+-}}(\mathbf{p}, \mathbf{q})\delta_{ss'}$	$-\frac{3}{8}V_{\pi^{+-}}(\mathbf{p}, \mathbf{q})\delta_{ss'}$

the positive energy component of the  $\pi$  to its negative energy component. The quark exchange overlaps  $\langle V_{14} \rangle$ ,  $\langle V_{25} \rangle$  and  $\langle V_{23} \rangle$ , include a linear combination of the spin singlet  $V_{\pi^{++}}$  and of the spin triplet  $V_{\rho^{++}}$ .

## 5.2 Flavour contributions

Table 4

Flavor contributions.  $\tau_N, \tau_{\pi}$  are, respectively, the isospin generators acting in I=1/2 and 1 isospin wave functions. The I represents the identity operator in flavor space

	F		D	
	$\phi^+\phi^+$	$\phi^-\phi^-$	$\phi^+\phi^+$	$\phi^-\phi^-$
$\langle E \rangle, \langle T_i \rangle$	$\frac{1}{2}I$	$\frac{1}{2}I$	$\frac{1}{2}I + \frac{2}{3}\tau_N \cdot \tau_{\pi}$	$\frac{1}{2}I - \frac{2}{3}\tau_N \cdot \tau_{\pi}$
$\langle V_{14} \rangle$	$\frac{1}{2}I$	$\frac{1}{2}I$	$\frac{1}{2}I + \frac{2}{3}\tau_N \cdot \tau_{\pi}$	$\frac{1}{2}I - \frac{2}{3}\tau_N \cdot \tau_{\pi}$
$\langle V_{25} \rangle$	$\frac{1}{2}I$	$\frac{1}{2}I$	$\frac{1}{2}I + \frac{2}{3}\tau_N \cdot \tau_{\pi}$	$\frac{1}{2}I - \frac{2}{3}\tau_N \cdot \tau_{\pi}$
$\langle V_{23} \rangle$	$\frac{1}{2}I + \tau_N \cdot \tau_{\pi}$	$\frac{1}{2}I - \tau_N \cdot \tau_{\pi}$	$\frac{1}{2}I - \frac{1}{3}\tau_N \cdot \tau_{\pi}$	$\frac{1}{2}I + \frac{1}{3}\tau_N \cdot \tau_{\pi}$
$\langle A_{15} \rangle$	$\frac{1}{2}I$	$\frac{1}{2}I$	$\frac{1}{2}I - \frac{2}{3}\tau_N \cdot \tau_{\pi}$	$\frac{1}{2}I + \frac{2}{3}\tau_N \cdot \tau_{\pi}$

In the case of the flavour diagrams with different energy-spin asymptotic states for the mesons contribute differently. As we have said the existence of negative

Table 5

Flavor contributions.  $\tau_\pi$  and  $\tau_\Delta$  are, respectively, the isospin generators acting in  $I=1$  and  $3/2$  isospin wave functions. The  $I$  represents the identity operator in flavor space

	$\Delta\pi$	
	$\phi^+\phi^+$	$\phi^-\phi^-$
$\langle E \rangle, \langle T_i \rangle$	$\frac{1}{2}I + \frac{1}{3}\tau_\Delta \cdot \tau_\pi$	$\frac{1}{2}I - \frac{1}{3}\tau_\Delta \cdot \tau_\pi$
$\langle V_{14} \rangle$	$\frac{1}{2}I + \frac{1}{3}\tau_\Delta \cdot \tau_\pi$	$\frac{1}{2}I - \frac{1}{3}\tau_\Delta \cdot \tau_\pi$
$\langle V_{25} \rangle$	$\frac{1}{2}I + \frac{1}{3}\tau_\Delta \cdot \tau_\pi$	$\frac{1}{2}I - \frac{1}{3}\tau_\Delta \cdot \tau_\pi$
$\langle V_{23} \rangle$	$\frac{1}{2}I + \frac{1}{3}\tau_\Delta \cdot \tau_\pi$	$\frac{1}{2}I - \frac{1}{3}\tau_\Delta \cdot \tau_\pi$
$\langle A_{15} \rangle$	$\frac{1}{2}I - \frac{1}{3}\tau_\Delta \cdot \tau_\pi$	$\frac{1}{2}I + \frac{1}{3}\tau_\Delta \cdot \tau_\pi$

Table 6

Nucleon Total Contribution. The upper (lower) sum/subtraction signs are associated with  $\phi^+ \otimes \phi^+$  ( $\phi^- \otimes \phi^-$ ).  $E^\pm = E_B \pm E_\pi$ , with  $E_B$  and  $E_\pi$  being the energy of the incoming baryon and pion

$\langle E \rangle, \langle T_i \rangle$	$\frac{1}{4}(I \pm \frac{2}{3}\tau_N \cdot \tau_\pi)(2T_1 + 2T_2 + T_5 - E^\pm)$
$\langle V_{14} \rangle$	$-\frac{1}{4}(I \pm \frac{2}{3}\tau_N \cdot \tau_\pi)V_\pi^{++}(\mathbf{p}, \mathbf{q})$
$\langle V_{25} \rangle$	$-\frac{1}{8}I V_\pi^{++}(\mathbf{p}, \mathbf{q}) - \frac{1}{8}(I \pm \frac{4}{3}\tau_N \cdot \tau_\pi)V_\rho^{++}(\mathbf{p}, \mathbf{q})$
$\langle V_{23} \rangle$	$\frac{1}{16}(I \pm 2\tau_N \cdot \tau_\pi)V_\pi^{++}(\mathbf{p}, \mathbf{q}) + \frac{1}{16}(I \mp \frac{2}{3}\tau_N \cdot \tau_\pi)V_\rho^{++}(\mathbf{p}, \mathbf{q})$
$\langle A_{15} \rangle$	$\frac{1}{4}(I \mp \frac{2}{3}\tau_N \cdot \tau_\pi)V_\pi^{+-}(\mathbf{p}, \mathbf{q})$

energy-spin  $\phi^-$  amounts to the doubling of diagrams of Fig. 2 each of them giving rise to two diagrams, one with  $\phi^+\phi^+$  mesonic asymptotic states and another with  $\phi^-\phi^-$  mesonic asymptotic states. No diagrams with  $\phi^+\phi^-$  are allowed.

We give the isospin traces in Tables 4 and 5 for  $N\pi$  and  $\Delta\pi$  in terms of the  $\phi^\pm$  content of the diagrams  $\langle E \rangle, \langle T_i \rangle, \langle V_{14} \rangle, \langle V_{23} \rangle$  and  $\langle A_{15} \rangle$ . As in the spin case we must distinguish between the  $F$  and  $D$  flavour components because the nucleon wave function mixes this components with the correspondent  $F$  and  $D$  spin. So the net result of considering negative energy amplitudes for the mesons is to double the entries in Table 4 for each of the flavours  $F$  and  $D$ . In this respect the  $\Delta\pi$  case is simpler and we can give final flavour results for  $\phi^+\phi^+$  and  $\phi^-\phi^-$ .

Next we can assemble the results of Tables 2, 3, 4 and 5 to obtain the final  $\pi - B$  results for colour $\times$ spin $\times$ flavour $\times$ momentum presented in Tables 6 and 7.

Table 7

Delta Total Contribution. The upper (lower) sum/subtraction signs are associated with  $\phi^+ \otimes \phi^+$  ( $\phi^- \otimes \phi^-$ ).

$\langle E \rangle, \langle T_i \rangle$	$\frac{1}{4}(I \pm \frac{2}{3}\tau_\Delta \cdot \tau_\pi)(2T_1 + 2T_2 + T_5 - E^\pm)$
$\langle V_{14} \rangle$	$-\frac{1}{4}(I \pm \frac{2}{3}\tau_\Delta \cdot \tau_\pi)V_\pi^{++}(\mathbf{p}, \mathbf{q})$
$\langle V_{25} \rangle$	$-\frac{1}{4}(I \pm \frac{2}{3}\tau_\Delta \cdot \tau_\pi)V_\rho^{++}(\mathbf{p}, \mathbf{q})$
$\langle V_{23} \rangle$	$\frac{1}{8}(I \pm \frac{2}{3}\tau_\Delta \cdot \tau_\pi)V_\rho^{++}(\mathbf{p}, \mathbf{q})$
$\langle A_{15} \rangle$	$\frac{1}{4}(I \mp \frac{2}{3}\tau_\Delta \cdot \tau_\pi)V_\pi^{+-}(\mathbf{p}, \mathbf{q})$

Finally integrating in the internal momenta  $p$ ,  $q$  and  $k$  we get for  $\mathcal{O}_{\pi-N}^{\text{RGM}}$

$$\begin{aligned}
\mathcal{O}_{\pi-N}^{\text{RGM}} = & \int \frac{d^3p}{(2\pi)^3} \frac{d^3q}{(2\pi)^3} \frac{d^3k}{(2\pi)^3} \\
& \left\{ \Psi(p, k)\phi^+(p) \frac{1}{4}A_1(2T_1 + 2T_2 + T_5 - E^+)\Psi(p, k)\phi^+(p) \delta^3(\mathbf{p} - \mathbf{q}) + \right. \\
& + \Psi(p, k)\Psi(p, k) \frac{1}{4} \left( A_1V_\pi^{++} + A_{-1}V_\pi^{+-} \right) \phi^+(q)\phi^+(q) + \\
& + \Psi(p, k)\phi^+(p) \frac{1}{8} \left( I V_\pi^{++} + A_2V_\rho^{++} \right) \Psi(q, k)\phi^+(q) + \\
& + \Psi(p, k)\phi^+(k) \frac{1}{16} \left( A_3V_\pi^{++} + A_{-1}V_\rho^{++} \right) \Psi(q, k)\phi^+(k) + \\
& + \Psi(p, k)\phi^-(p) \frac{1}{4}A_{-1}(2T_1 + 2T_2 + T_5 - E^-)\Psi(p, k)\phi^-(p) \delta^3(\mathbf{p} - \mathbf{q}) + \\
& + \Psi(p, k)\Psi(p, k) \frac{1}{4} \left( A_{-1}V_\pi^{++} + A_1V_\pi^{+-} \right) \phi^-(q)\phi^-(q) + \\
& + \Psi(p, k)\phi^-(p) \frac{1}{8} \left( I V_\pi^{++} + A_{-2}V_\rho^{++} \right) \Psi(q, k)\phi^-(q) + \\
& \left. + \Psi(p, k)\phi^-(k) \frac{1}{16} \left( A_{-3}V_\pi^{++} + A_1V_\rho^{++} \right) \Psi(q, k)\phi^-(k) \right\} , \tag{26}
\end{aligned}$$

with  $A_n = I + \frac{2}{3}n\tau_N \cdot \tau_\pi$ .

Similarly for the  $\pi\Delta - \pi\Delta$  overlaps we get

$$\begin{aligned}
\mathcal{O}_{\pi-\Delta}^{\text{RGM}} = & \int \frac{d^3p}{(2\pi)^3} \frac{d^3q}{(2\pi)^3} \frac{d^3k}{(2\pi)^3} \\
& \left\{ \Psi_{\Delta}(p, k) \phi^+(p) \frac{1}{4} A_1 (2T_1 + 2T_2 + T_5 - E^+) \Psi_{\Delta}(p, k) \phi^+(p) \delta^3(\mathbf{p} - \mathbf{q}) + \right. \\
& + \Psi_{\Delta}(p, k) \Psi_{\Delta}(p, k) \left( \frac{1}{4} A_1 V_{\pi}^{++} + \frac{1}{4} A_{-1} V_{\pi}^{+-} \right) \phi^+(q) \phi^+(q) + \\
& + \Psi_{\Delta}(p, k) \phi^+(p) \left( \frac{1}{4} A_1 V_{\rho}^{++} \right) \Psi_{\Delta}(q, k) \phi^+(q) + \\
& + \Psi_{\Delta}(p, k) \phi^+(k) \left( \frac{1}{8} A_1 V_{\rho}^{++} \right) \Psi_{\Delta}(q, k) \phi^+(k) + \\
& + \Psi_{\Delta}(p, k) \phi^-(p) \frac{1}{4} A_{-1} (2T_1 + 2T_2 + T_5 - E^-) \Psi_{\Delta}(p, k) \phi^-(p) \delta^3(\mathbf{p} - \mathbf{q}) + \\
& + \Psi_{\Delta}(p, k) \Psi_{\Delta}(p, k) \left( \frac{1}{4} A_{-1} V_{\pi}^{++} + \frac{1}{4} A_1 V_{\pi}^{+-} \right) \phi^-(q) \phi^-(q) + \\
& + \Psi_{\Delta}(p, k) \phi^-(p) \left( \frac{1}{4} A_{-1} V_{\rho}^{++} \right) \Psi_{\Delta}(q, k) \phi^-(q) + \\
& \left. + \Psi_{\Delta}(p, k) \phi^-(k) \left( \frac{1}{8} A_{-1} V_{\rho}^{++} \right) \Psi_{\Delta}(q, k) \phi^-(k) \right\} .
\end{aligned} \tag{27}$$

It is a matter of a simple calculation, to rewrite Eqs. (26) and (27) in order to bring forward the explicit dependence on the matrix elements  $\mathcal{H}_{\pi}$ ,  $\mathcal{H}_N$  and  $\mathcal{H}_{\Delta}$ .

As an example let us consider the  $\pi - N$  case. We use the following general identity

$$\begin{aligned}
& \int \frac{d^3p}{(2\pi)^3} \int \frac{d^3p'}{(2\pi)^3} \chi(\mathbf{p}) (2T + V_{\pi}^{++}(\mathbf{p}, \mathbf{p}') + V_{\pi}^{+-}(\mathbf{p}, \mathbf{p}')) \zeta(\mathbf{p}') = \\
& = \frac{1}{2} \int \frac{d^3p}{(2\pi)^3} \int \frac{d^3p'}{(2\pi)^3} \left[ \chi(\mathbf{p}), \chi(\mathbf{p}) \right] \mathcal{H}_{\pi} \begin{bmatrix} \zeta(\mathbf{p}') \\ \zeta(\mathbf{p}') \end{bmatrix} ,
\end{aligned} \tag{28}$$

with  $\chi$  and  $\xi$  being arbitrary functions, together with the definition of  $\mathcal{H}_N$  and  $\mathcal{H}_\Delta$  (see Eqs. (25)), to cast Eq. (26) as

$$\begin{aligned}
\mathcal{O}_{\pi-N}^{\text{RGM}} = & \sum_{\alpha=\pm} \int \frac{d^3p}{(2\pi)^3} \frac{d^3q}{(2\pi)^3} \frac{d^3k}{(2\pi)^3} \\
& \left\{ -\Psi(p, k) \phi^\alpha(p) \frac{E^\alpha}{4} \left( I + \alpha \frac{2}{3} \tau_N \cdot \tau_\pi \right) \Psi(p, k) \phi^\alpha(p) \delta^3(\mathbf{p} - \mathbf{q}) + \right. \\
& + \frac{1}{8} \left[ \Psi(p, k) \Psi(p, k), \Psi(p, k) \Psi(p, k) \right] \mathcal{H}_\pi \left( I - \alpha \frac{2}{3} \tau_N \cdot \tau_\pi \right) \begin{bmatrix} \phi^\alpha(q) \phi^\alpha(q) \\ \phi^\alpha(q) \phi^\alpha(q) \end{bmatrix} + \\
& + \Psi(p, k) \Psi(p, k) \frac{1}{3} (2\mathcal{H}_N - \mathcal{H}_\Delta) \alpha \frac{2}{3} \tau_N \cdot \tau_\pi \phi^\alpha(q) \phi^\alpha(q) + \\
& + \Psi(p, k) \phi^\alpha(p) \frac{1}{6} \left( \mathcal{H}_N I + \mathcal{H}_\Delta \alpha \frac{2}{3} \tau_N \cdot \tau_\pi \right) \Psi(q, k) \phi^\alpha(q) + \\
& \left. + \Psi(p, k) \phi^\alpha(k) \frac{1}{12} \left( \mathcal{H}_N I + (3\mathcal{H}_N - 2\mathcal{H}_\Delta) \alpha \frac{2}{3} \tau_N \cdot \tau_\pi \right) \Psi(q, k) \phi^\alpha(k) \right\} . \tag{29}
\end{aligned}$$

Finally we use the spectral decomposition of  $\mathcal{H}_\pi$ ,  $\mathcal{H}_N$  and  $\mathcal{H}_\Delta$ ,

$$\begin{aligned}
H_\pi = & \sum_{\pi^*} \sigma_3 \begin{bmatrix} |\phi_{\pi^*}^+\rangle \\ |\phi_{\pi^*}^-\rangle \end{bmatrix} M_{\pi^*} \left[ \langle \phi_{\pi^*}^+ | \langle \phi_{\pi^*}^- | \right] \sigma_3 + \\
& + \sigma_3 \begin{bmatrix} |\phi_{\pi^*}^-\rangle \\ |\phi_{\pi^*}^+\rangle \end{bmatrix} M_{\pi^*} \left[ \langle \phi_{\pi^*}^- | \langle \phi_{\pi^*}^+ | \right] \sigma_3 , \tag{30} \\
H_N = & \sum_{N^*} |\psi_{N^*}\rangle M_{N^*} \langle \psi_{N^*}| , \\
H_\Delta = & \sum_{\Delta^*} |\psi_{\Delta^*}\rangle M_{\Delta^*} \langle \psi_{\Delta^*}| ,
\end{aligned}$$

which are a direct consequence of Eq. (25), to obtain for  $\mathcal{O}_{\pi-B}^{\text{RGM}}$

$$\begin{aligned}
\mathcal{O}_{\pi-N}^{\text{RGM}} = & \sum_{\alpha=\pm} \left\{ -I_0^\alpha \frac{E^\alpha}{4} \left( I + \alpha \frac{2}{3} \tau_N \cdot \tau_\pi \right) + \frac{1}{8} I_4 M_\pi \left( I - \alpha \frac{2}{3} \tau_N \cdot \tau_\pi \right) I_5^\alpha + \right. \\
& + \frac{1}{3} I_1 (2M_N - M_\Delta) \alpha \frac{2}{3} \tau_N \cdot \tau_\pi I_2^\alpha + \frac{1}{6} I_3^\alpha \left( M_N I + M_\Delta \alpha \frac{2}{3} \tau_N \cdot \tau_\pi \right) I_3^\alpha + \\
& \left. + \frac{1}{12} I_6 \left( M_N I + (3M_N - 2M_\Delta) \alpha \frac{2}{3} \tau_N \cdot \tau_\pi \right) I_6 \right\} , \tag{31}
\end{aligned}$$

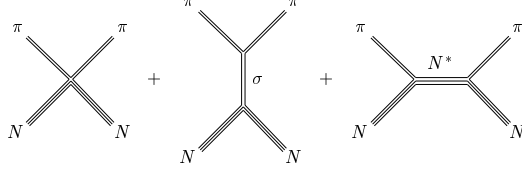


Fig. 6. Classes of diagrams in  $\pi - B$  scattering

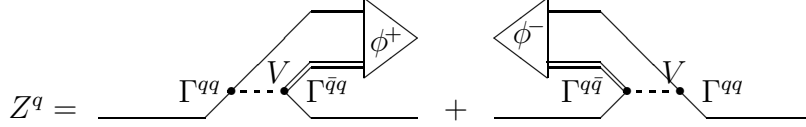


Fig. 7.  $Z^q$  annihilation of a meson in a quark line

with

$$\begin{aligned}
I_0^\pm &= \int \frac{d^3p}{(2\pi)^3} \Psi_B(p) \Psi_B(p) \phi^\pm(p) \phi^\pm(p), \\
I_1 &= \int \frac{d^3p}{(2\pi)^3} \Psi_B(p) \Psi_B(p) \Psi_{B'}(p), \quad I_2^\pm = \int \frac{d^3p}{(2\pi)^3} \phi^\pm(p) \phi^\pm(p) \Psi_{B'}(p), \\
I_3^\pm &= \int \frac{d^3p}{(2\pi)^3} \Psi_B(p) \phi^\pm(p) \Psi_{B'}, \quad I_4 = \int \frac{d^3p}{(2\pi)^3} \Psi_B(p) \Psi_B(p) (\phi^+(p) - \phi^-(p)), \\
I_5^\pm &= \int \frac{d^3p}{(2\pi)^3} \phi^\pm(p) \phi^\pm(p) (\phi^+(p) - \phi^-(p)), \quad I_6 = \sqrt{\frac{3}{f_\pi^2 m_\pi}} \int \frac{d^3p}{(2\pi)^3} \Psi_B(p) \Psi_{B'}(p).
\end{aligned} \tag{32}$$

We can deal with  $\pi - \Delta$  along similar lines. Here we only quote the result:

$$\begin{aligned}
\mathcal{O}_{\pi-\Delta}^{\text{RGM}} &= \sum_{\alpha=\pm} \left\{ -I_0^\alpha \frac{E^\alpha}{4} \left( I + \alpha \frac{2}{3} \tau_\Delta \cdot \tau_\pi \right) + \frac{1}{8} I_4 M_\pi \left( I - \alpha \frac{2}{3} \tau_\Delta \cdot \tau_\pi \right) I_5^\alpha + \right. \\
&\quad \left. + \frac{1}{3} I_1 (2M_N - M_\Delta) \alpha \frac{2}{3} \tau_\Delta \cdot \tau_\pi I_2^\alpha + \frac{1}{6} I_3^\alpha M_\Delta \left( I + \alpha \frac{2}{3} \tau_\Delta \cdot \tau_\pi \right) I_3^\alpha + \right. \\
&\quad \left. + \frac{1}{12} I_6 M_\Delta \left( I + \alpha \frac{2}{3} \tau_\Delta \cdot \tau_\pi \right) I_6 \right\}.
\end{aligned} \tag{33}$$

We have succeeded in writing  $\mathcal{O}_{\pi-B}^{\text{RGM}}$  in terms of hadron masses and geometric overlaps only. Any explicit dependence on the microscopic quark kernel  $K$  as disappeared. The above formulas (31) and (33) are kernel independent. In the next section we are going to evaluate the geometrical overlaps  $I$ 's of Eq. (32) in the point-like limit approximation.

## 6 The point like limit

In this paper we follow closely the work done in the  $\pi - \pi$  case [2]. There it was shown, for any microscopic model complying with chiral symmetry, that in order to calculate  $\pi - \pi$  scattering lengths it is sufficient to consider the point-like limit,

$$S(k) \longrightarrow 1 . \quad (34)$$

In this limit only contact diagrams contribute to  $\pi - \pi$   $T$  matrix. This is clearly seen if we compute [14,17,18] the coupling of a meson to a single quark line with the  $Z^q$  annihilation diagrams depicted in Fig. 7. In this limit, the vertices present in Fig. 7, which represent the integral

$$\begin{aligned} Z_{s_1, s_2}^q(p) = & \sum_{s_3, s_4} \int \frac{d^3 p'}{(2\pi)^3} \Gamma_{s_1, s_3}^{qq}(p, p') V(p - p') \Gamma_{s_2, s_4}^{\bar{q}q}(p', p) \phi_{s_3, s_4}^+(p') + \\ & + \sum_{s_3, s_4} \int \frac{d^3 p'}{(2\pi)^3} \Gamma_{s_1, s_3}^{q\bar{q}}(p, p') V(p - p') \Gamma_{s_2, s_4}^{q\bar{q}}(p', p) \phi_{s_3, s_4}^-(p') , \end{aligned} \quad (35)$$

vanish. Assumption (34) implies the vanishing of the products of vertices,

$$\begin{aligned} \Gamma^{qq} \Gamma^{\bar{q}q} & \rightarrow 0 , & \Gamma^{q\bar{q}} \Gamma^{qq} & \rightarrow 0 , \\ \Gamma^{\bar{q}q} \Gamma^{\bar{q}q} & \rightarrow 0 , & \Gamma^{q\bar{q}} \Gamma^{q\bar{q}} & \rightarrow 0 . \end{aligned} \quad (36)$$

In the class of models embodied by Eq. (1)  $Z^q$  (and  $Z^{\bar{q}}$ ) are the microscopic sources of intermediate hadronic exchange so that, in this limit, diagrams which do not belong to the class of contact diagrams vanish. When leaving this limit both classes of diagrams contribute to  $T_{\pi-\pi}$  matrix, but then chiral symmetry forces cancellations among diagrams belonging to each of these two different classes, so that the  $T_{\pi-\pi}$  transition matrix remains formally invariant. This cancellation is clearly seen in the sigma model calculation of  $\pi - \pi$  scattering [29] where the X shaped diagram of the contact four  $\pi$  coupling and the H shaped diagram of the sigma meson exchange miraculously cancel and this provides the small physical result. This result is encoded by the existence of the Adler zeroes [30] which are present whenever a low energy pion couples to hadrons. In references [2,3] we have shown this cancellation for microscopic models defined for the class of Hamiltonians of Eq. (1). As a byproduct it was also shown that the transition matrix  $T_{\pi-\pi}$  is formally independent of the quark microscopic kernel  $K$ . In fact  $T_{\pi-\pi}$  was shown to depend explicitly only on physical masses  $m_\pi$  and wave-function normalizations  $f_\pi$ . So that any dependence on the quark kernel  $K$  is buried into the masses and normalization constants dependence on  $K$ . Therefore we were allowed, in order to find the  $T_{\pi-\pi}$  formula in terms of  $m_\pi$  and  $f_\pi$  to choose a kernel consistent to  $S(k) \rightarrow 1$ . In this paper we follow the prescription of  $S(k) \rightarrow 1$  and therefore we will only consider contact diagrams.

The integrals  $I$  of Eq. (32) are particularly simple to do in the point like limit. In Eqs. (31) and (33), the only relevant combinations of  $I$ 's we need to be concerned with, have, up to the first order in  $\xi = (\phi^+ - \phi^-)/2a$ , the following point like limits

$$\begin{aligned}
I_0^+ + I_0^- &= \int \frac{d^3p}{(2\pi)^3} \Psi_B \Psi_B \phi^+ \phi^+ + \int \frac{d^3p}{(2\pi)^3} \Psi_B \Psi_B \phi^- \phi^- \\
&= \frac{3}{f_\pi^2 M_\pi} \int \frac{d^3p}{(2\pi)^3} \Psi_B \Psi_B S^2 + \frac{4}{3} f_\pi^2 M_\pi \int \frac{d^3p}{(2\pi)^3} \Psi_B \Psi_B \xi^2 \\
&\xrightarrow{S \rightarrow 1} \frac{3}{f_\pi^2 M_\pi} \int \frac{d^3p}{(2\pi)^3} \Psi_B \Psi_B = \frac{3}{f_\pi^2 M_\pi} \\
I_0^+ - I_0^- &= \int \frac{d^3p}{(2\pi)^3} \Psi_B \Psi_B \phi^+ \phi^+ - \int \frac{d^3p}{(2\pi)^3} \Psi_B \Psi_B \phi^- \phi^- \\
&= 4 \int \frac{d^3p}{(2\pi)^3} \Psi_B \Psi_B S \frac{1}{2a} (\phi^+ - \phi^-) \\
&\xrightarrow{S \rightarrow 1} \frac{1}{\mathcal{N}^2} 4 \int \frac{d^3p}{(2\pi)^3} S \frac{1}{2a} (\phi^+ - \phi^-) = \frac{1}{\mathcal{N}^2}
\end{aligned} \tag{37}$$

$$\begin{aligned}
\{I_1 I_2^+ + I_1 I_2^-, I_1 I_2^+ - I_1 I_2^-\} &\xrightarrow{S \rightarrow 1} \left\{ \frac{3}{f_\pi^2 M_\pi}, \frac{1}{\mathcal{N}^2} \right\} \\
\{I_3^+ I_3^+ + I_3^- I_3^-, I_3^+ I_3^+ - I_3^- I_3^-\} &\xrightarrow{S \rightarrow 1} \left\{ \frac{3}{f_\pi^2 M_\pi}, \frac{1}{\mathcal{N}^2} \right\} \\
\{I_6 I_6 + I_6 I_6, I_6 I_6 - I_6 I_6\} &\xrightarrow{S \rightarrow 1} \left\{ \frac{3}{f_\pi^2 M_\pi}, 0 \right\} \\
\{I_4 I_5^+ + I_4 I_5^-, I_4 I_5^+ - I_4 I_5^-\} &\xrightarrow{S \rightarrow 1} \{ \mathcal{O}(M_\pi), \mathcal{O}(M_\pi) \}
\end{aligned}$$

In order to derive the limits of Eq. (37), Eqs. (15), (16) and (24) were used. The last entry of Eq. (37) presents combinations of the  $I$ 's which are of the order  $M_\pi$ . Because we are interested in scattering lengths evaluated to order zero in  $M_\pi$  these combinations will not be considered.

Using Eq. (37) we can further simplify  $\mathcal{O}_{\pi-B}^{\text{RGM}}$  noticing that due to energy conservation  $E_{\pi B}^\pm = M_B \pm M_\pi$ , the following combination

$$3 I \frac{-E_{\pi B}^+ - E_{\pi B}^- + 2M_B}{8f_\pi^2 M_\pi} = \mathcal{O}(M_\pi) . \tag{38}$$

is of order  $M_\pi$ . Therefore it will be discarded for the same reasons as before.

To zero order in  $M_\pi$ , only the  $\tau_B \cdot \tau_\pi$  terms survive, and the total overlap kernel  $\mathcal{O}_{\pi-B}^{\text{RGM}}$  turns out to be quite simple,

$$\mathcal{O}_{\pi-B}^{\text{RGM}} = \frac{4M_N - 2M_\Delta}{9\mathcal{N}^2} \tau_B \cdot \tau_\pi + \mathcal{O}(M_\pi) . \tag{39}$$

We finally get the desired scattering lengths, see Eq. (9), in a compact notation,

$$a_{\pi B} = -\frac{M_\pi}{2\pi} \frac{4M_N - 2M_\Delta}{9\mathcal{N}^2} \tau_B \cdot \tau_\pi + \mathcal{O}(M_\pi^2) . \quad (40)$$

The scattering lengths vanish in the chiral limit of a vanishing quark mass  $M_\pi \rightarrow 0$ , and this complies with the Adler zero [29,30] .

## 7 Numerical results and Conclusion

We have a free parameter, the  $N$  and  $\Delta$  normalization that  $\mathcal{N}$  needs to be fixed. To this effect we can use the experimental value for the  $a_{\pi N}\{I = 1/2\}$  scattering length,

$$a_{\pi N}^{exp}\{I = 1/2\} = (0.171 \pm 0.005)M_\pi^{-1} , \quad (41)$$

to fix  $\mathcal{N}$ . We obtain  $\mathcal{N} = 1580MeV^{-3/2}$ , corresponding to a nucleon size of 0.4 fm. Equipped with this value we predict the following values for

$$\begin{aligned} a_{\pi N}\{I = 3/2\} &= -0.086M_\pi^{-1} & [a_{\pi N}^{exp}\{I = 3/2\} &= -(0.088 \pm 0.004)M_\pi^{-1}] , \\ a_{\pi\Delta}\{I = 1/2\} &= 0.429M_\pi^{-1} , \\ a_{\pi\Delta}\{I = 3/2\} &= 0.172M_\pi^{-1} , \\ a_{\pi\Delta}\{I = 5/2\} &= -0.258M_\pi^{-1} . \end{aligned} \quad (42)$$

Although it is difficult to measure directly the  $\pi - \Delta$  scattering lengths because the  $\Delta$  is quite unstable, the  $\pi - \Delta$  coupling may be determined indirectly in the same way as the  $N - \Delta$  scattering lengths are determined in Ref. [31]. We stress that the QM provides the correct framework to derive the  $\pi - \Delta$  scattering lengths. For instance it would be hard to derive the  $\pi - \Delta$  scattering lengths in the framework of effective hadronic models.

In particular we predict that the different scattering lengths of the  $\pi$  in s-wave baryons are exactly proportional with remarkable integer factors,

$$a_{\pi N, I=\frac{1}{2}} : a_{\pi N, I=\frac{3}{2}} : a_{\pi\Delta, I=\frac{1}{2}} : a_{\pi\Delta, I=\frac{3}{2}} : a_{\pi\Delta, I=\frac{5}{2}} = 2 : -1 : 5 : 2 : -3 . \quad (43)$$

The work of G. M. Marques is supported by Fundação para a Ciência e a Tecnologia under the grant SFRH/BD/984/2000.

## A Traces

In this appendix the computation of the color, spin and flavor traces are detailed. There are different equivalent methods to compute these standard traces.

### A.1 color

The color traces are the most straightforward to calculate. The baryon color wave-function is a simple  $\epsilon^{abc}/\sqrt{6}$  and the meson a  $\delta^{ab}/\sqrt{3}$ . The interaction has the well known structure  $\lambda^{ab}/2$ . For instance the pion Bethe-Salpeter color factor 4/3 of Eq. (13) is calculated in the following way

$$\frac{\delta_{ij}}{\sqrt{3}} \frac{\lambda_{ik}^a}{2} \frac{\delta_{kl}}{\sqrt{3}} \frac{\lambda_{jl}^b}{2} = \frac{1}{12} Tr\{\boldsymbol{\lambda} \cdot \boldsymbol{\lambda}\} = \frac{4}{3}. \quad (\text{A.1})$$

For the baryons the color factor -2/3 of Eqs. (19), (20) and (21) comes from

$$\frac{\epsilon_{ijk}}{\sqrt{6}} \frac{\lambda_{il}^a}{2} \frac{\epsilon_{lmk}}{\sqrt{6}} \frac{\lambda_{jm}^b}{2} = \frac{1}{24} (Tr\{\boldsymbol{\lambda}\} \cdot Tr\{\boldsymbol{\lambda}\} - Tr\{\boldsymbol{\lambda} \cdot \boldsymbol{\lambda}\}) = -\frac{2}{3} \quad (\text{A.2})$$

In Table 2 we present the results for the diagrams of Fig. 2.

### A.2 spin

For the spin our method relies on the Pauli matrices  $\sigma_i$ .

The spin structures of  $\pi$ ,  $N$  and  $\Delta$  wave functions, together with the spin vector structure  $\rho$ , later needed in the calculations, can be written as

$$\begin{aligned} \Sigma^\pi &= (i\sigma_2/\sqrt{2})_{ab}; & \Sigma_{\mathbf{s}}^\rho &= [\boldsymbol{\sigma}i\sigma_2/\sqrt{2}]_{ab} \cdot \mathbf{v}_{\mathbf{s}}; & \Sigma_{\mathbf{s}}^\Delta &= [\boldsymbol{\sigma}i\sigma_2/\sqrt{2}]_{ab} \cdot \mathbf{w}_{cs}; \\ \Sigma_{\mathbf{s}}^{N^F} &= (i\sigma_2/\sqrt{2})_{ab} \delta_{cs}; & \Sigma_{\mathbf{s}}^{N^D} &= (1/\sqrt{3}) [\boldsymbol{\sigma}i\sigma_2/\sqrt{2}]_{ab} \cdot \boldsymbol{\sigma}_{cs} \end{aligned} \quad (\text{A.3})$$

where  $a$ ,  $b$  and  $c$  stand for the quarks individual spin, whereas  $\mathbf{s}$  stands for the **total** spin of the meson or baryon under consideration. For example, we have

$$\left[ \begin{array}{c} \uparrow \downarrow \\ \downarrow \uparrow \end{array} \right] \Sigma^\pi \left[ \begin{array}{c} \uparrow \\ \downarrow \end{array} \right] = \frac{1}{\sqrt{2}} (\uparrow\downarrow - \downarrow\uparrow). \quad (\text{A.4})$$

The vectors  $\mathbf{v}_s$  and  $\mathbf{w}_{cs}$ , are given by,

$$\begin{aligned}\mathbf{v}_1 &= \left(-1/\sqrt{2}, -i/\sqrt{2}, 0\right), \quad \mathbf{v}_0 = (0, 0, -1), \quad \mathbf{v}_{-1} = \left(1/\sqrt{2}, -i/\sqrt{2}, 0\right), \\ \mathbf{w}_{c\frac{3}{2}} &= \mathbf{v}_1 \delta_{c\frac{1}{2}}, \quad \mathbf{w}_{c\frac{1}{2}} = 1/\sqrt{3} \mathbf{v}_1 \sigma_{c\frac{1}{2}}^- + \sqrt{2/3} \mathbf{v}_0 \delta_{c\frac{1}{2}}, \\ \mathbf{w}_{c-\frac{1}{2}} &= 1/\sqrt{3} \mathbf{v}_{-1} \sigma_{c-\frac{1}{2}}^+ + \sqrt{2/3} \mathbf{v}_0 \delta_{c-\frac{1}{2}}, \quad \mathbf{w}_{c-\frac{3}{2}} = \mathbf{v}_{-1} \delta_{c-\frac{1}{2}}.\end{aligned}\tag{A.5}$$

They have the following properties,

$$\begin{aligned}v_s^{i\dagger} v_{s'}^j &= \delta^{ij} \delta_{ss'} - (J^j J^i)_{ss'}, \\ w_{sc}^{i\dagger} w_{cs'}^j &= \frac{3}{4} \delta^{ij} \delta_{ss'} - \frac{1}{3} (J^i J^j)_{ss'} + \frac{i}{2} \epsilon^{ijk} J_{ss'}^k.\end{aligned}\tag{A.6}$$

where the  $J$ 's are the spin 1 SU(2) generating matrices in the case of the  $v$ 's relation and the spin 3/2 SU(2) generating matrices in the case of the  $w$ 's relation. When we contract  $i$  with  $j$  we have simply

$$v_s^{i\dagger} v_{s'}^i = w_{sc}^{i\dagger} w_{cs'}^i = \delta_{ss'}.\tag{A.7}$$

The importance of the above spin functions lies in the fact that they map the quark spin content of a given bound state to the total spin of that bound state. Once this map is achieved it is a matter of straightforward calculations to obtain the diagrammatic traces. The results are presented in table A.1. For instance for the spin traces which contribute to the RGM  $\langle E \rangle$  and  $\langle V_{24} \rangle$  overlap diagrams the computation is

$$\begin{aligned}\langle E \rangle_{spin} &= Tr \{ \Sigma_s^B \cdot \Sigma_{s'}^{B\dagger} \cdot \Sigma^\pi \cdot \Sigma^{\pi\dagger} \} = \\ &= -\frac{1}{2} \delta_{ss'},\end{aligned}\tag{A.8}$$

$$\begin{aligned}\langle V_{24} \rangle_{spin} &= Tr \{ \Sigma_s^B \cdot \Sigma_{s'}^{B\dagger} \cdot \Gamma^{qq} \cdot \Sigma^\pi \cdot \Sigma^{\pi\dagger} \cdot \Gamma^{qq} \} V(\mathbf{p} - \mathbf{p}') = \\ &= \frac{1}{2} Tr \{ \Sigma_s^B \cdot \Sigma_{s'}^{B\dagger} \cdot \Gamma^{qq} \cdot \Gamma^{qq} \} V(\mathbf{p} - \mathbf{p}') = \\ &= -\frac{3}{8} V_\pi^{++}(\mathbf{p}, \mathbf{p}') \delta_{ss'}.\end{aligned}\tag{A.9}$$

where the super-index  $B$  stands for the corresponding baryon which may be the  $F$  component of the nucleon, the  $D$  component of the nucleon or the Delta.

### A.3 flavor

In the isospin case we use  $\tau_i$  as the Pauli matrices.

Table A.1  
Spin contributions

$\langle E \rangle, \langle T_i \rangle$	$Tr\{\Sigma_s^B \cdot \Sigma_{s'}^{B\dagger} \cdot \Sigma^\pi \cdot \Sigma^{\pi\dagger}\}$
$\langle V_{14} \rangle$	$Tr\{\Sigma_s^B \cdot \Sigma_{s'}^{B\dagger} \cdot \Gamma^{qq} \cdot \Sigma^\pi \cdot \Sigma^{\pi\dagger} \cdot \Gamma^{qq}\}V(\mathbf{p} - \mathbf{q})$
$\langle V_{25} \rangle$	$Tr\{\Sigma_s^B \cdot \Gamma^{qq} \cdot \Sigma_{s'}^{B\dagger} \cdot \Sigma^\pi \cdot \Gamma^{\bar{q}\bar{q}} \cdot \Sigma^{\pi\dagger}\}V(\mathbf{p} - \mathbf{q})$
$\langle V_{23} \rangle$	$\frac{1}{2}Tr\{\Sigma_s^B \cdot \Gamma^{qq} \cdot \Sigma_{s'}^{B\dagger} \cdot \Gamma^{qq}\}V(\mathbf{p} - \mathbf{q})$
$\langle A_{15} \rangle$	$Tr\{\Sigma_s^B \cdot \Sigma_{s'}^{B\dagger} \cdot \Gamma^{\bar{q}\bar{q}} \cdot \Sigma^{\pi\dagger} \cdot \Sigma^\pi \cdot \Gamma^{\bar{q}\bar{q}}\}V(\mathbf{p} - \mathbf{q})$

For  $\pi - N$  we have the cases of isospin 3/2 and 1/2.

$$\begin{aligned}
(I = 3/2) : & \quad p\pi^+, \frac{1}{\sqrt{3}}(n\pi^+ + \sqrt{2}p\pi^0), \frac{1}{\sqrt{3}}(\sqrt{2}n\pi^0 + p\pi^-), n\pi^- \\
(I = 1/2) : & \quad \frac{1}{\sqrt{3}}(\sqrt{2}n\pi^+ - p\pi^0), \frac{1}{\sqrt{3}}(n\pi^0 - \sqrt{2}p\pi^-)
\end{aligned} \tag{A.10}$$

The isospin contribution of any diagram must be a linear combination of the identity and  $\tau_N \cdot \tau_\pi$ , where

$$\tau_N \cdot \tau_\pi = \frac{1}{2}((\tau_\pi + \tau_N)^2 - \tau_\pi^2 - \tau_N^2) = \frac{1}{2}(I(I+1) - 2 - \frac{3}{4}). \tag{A.11}$$

The computation of these contributions was done for each diagram and each multiplet element. The results are presented in Table A.2.

In the same way for  $\Delta - \pi$  we have isospin 5/2, 3/2 and 1/2.

$$\begin{aligned}
(I = 5/2) : & \quad \Delta^{++}\pi^+, \frac{1}{\sqrt{5}}(\sqrt{2}\Delta^{++}\pi^0 + \sqrt{3}\Delta^+\pi^+), \frac{1}{\sqrt{10}}(\Delta^{++}\pi^- + \sqrt{6}\Delta^+\pi^0 + \sqrt{3}\Delta^0\pi^+) \\
& \quad \frac{1}{\sqrt{10}}(\sqrt{3}\Delta^+\pi^- + \sqrt{6}\Delta^0\pi^0 + \Delta^-\pi^+), \frac{1}{\sqrt{5}}(\sqrt{3}\Delta^0\pi^- + \sqrt{2}\Delta^-\pi^0), \Delta^-\pi^- \\
(I = 3/2) : & \quad \frac{1}{\sqrt{5}}(\sqrt{3}\Delta^{++}\pi^0 - \sqrt{2}\Delta^+\pi^+), \frac{1}{\sqrt{15}}(\sqrt{2}\Delta^{++}\pi^- + \Delta^+\pi^0 - \sqrt{8}\Delta^0\pi^+), \\
& \quad \frac{1}{\sqrt{15}}(\sqrt{8}\Delta^+\pi^- - \Delta^0\pi^0 - \sqrt{2}\Delta^-\pi^+), \frac{1}{\sqrt{5}}(\sqrt{2}\Delta^0\pi^- - \sqrt{3}\Delta^-\pi^0) \\
(I = 1/2) : & \quad \frac{1}{\sqrt{6}}(\sqrt{3}\Delta^{++}\pi^- - \sqrt{2}\Delta^+\pi^0 + \Delta^0\pi^+), \frac{1}{\sqrt{6}}(\Delta^+\pi^- - \sqrt{2}\Delta^0\pi^0 + \sqrt{3}\Delta^-\pi^+)
\end{aligned} \tag{A.12}$$

In this case the isospin contributions must be a linear combination of the

identity,  $\tau_\Delta \cdot \tau_\pi$  and  $(\tau_\Delta \cdot \tau_\pi)^2$ , once more where

$$\tau_\Delta \cdot \tau_\pi = \frac{1}{2}((\tau_\pi + \tau_\Delta)^2 - \tau_\pi^2 - \tau_\Delta^2) = \frac{1}{2}(I(I+1) - 2 - \frac{15}{4}). \quad (\text{A.13})$$

Table A.2 includes also the isospin structures of each diagram for  $\Delta - \pi$  scattering.

Table A.2

Flavor contributions.  $\tau_N$ ,  $\tau_\pi$  and  $\tau_\Delta$  are, respectively, the isospin generators acting in I= 1/2, 1 and 3/2 isospin wave functions. The I represents the identity operator in flavor space

	$N\pi$		$\Delta\pi$
	F	D	
$\langle E \rangle, \langle T_i \rangle$	$\frac{1}{2}I$	$\frac{1}{2}I + \frac{2}{3}\tau_N \cdot \tau_\pi$	$\frac{1}{2}I + \frac{1}{3}\tau_\Delta \cdot \tau_\pi$
$\langle V_{14} \rangle$	$\frac{1}{2}I$	$\frac{1}{2}I + \frac{2}{3}\tau_N \cdot \tau_\pi$	$\frac{1}{2}I + \frac{1}{3}\tau_\Delta \cdot \tau_\pi$
$\langle V_{25} \rangle$	$\frac{1}{2}I$	$\frac{1}{2}I + \frac{2}{3}\tau_N \cdot \tau_\pi$	$\frac{1}{2}I + \frac{1}{3}\tau_\Delta \cdot \tau_\pi$
$\langle V_{23} \rangle$	$\frac{1}{2}I + \tau_N \cdot \tau_\pi$	$\frac{1}{2}I - \frac{1}{3}\tau_N \cdot \tau_\pi$	$\frac{1}{2}I + \frac{1}{3}\tau_\Delta \cdot \tau_\pi$
$\langle A_{15} \rangle$	$\frac{1}{2}I$	$\frac{1}{2}I - \frac{2}{3}\tau_N \cdot \tau_\pi$	$\frac{1}{2}I - \frac{1}{3}\tau_\Delta \cdot \tau_\pi$

## References

- [1] S. Weinberg, Phys. Rev. Lett. **17** (1966) 616.
- [2] P. Bicudo, S. Cotanch, F. Llanes-Estrada, P. Maris, E. Ribeiro and A. Szczepaniak, Phys. Rev. D **65** (2002) 076008 [arXiv:hep-ph/0112015].
- [3] P. Bicudo, Phys. Rev. C **67** (2003) 035201.
- [4] J. Ribeiro, Nuc. Phys. A **689**,247c (2001).
- [5] A. Chodos, R.L. Jaffe, K. Johnson, C.B. Thorn, and V.F. Weisskopf, Phys. Rev. D **9**, 3471 (1974); A. Chodos, R.L. Jaffe, K. Johnson, and C.B. Thorn, *ibid* **10**, 2599 (1974); T.A. de Grand, R.L. Jaffe, K. Johnson, and J. Kiskis, *ibid* **12**, 2060 (1975).
- [6] A. Chodos and C.B. Thorn, Phys. Rev. D. **12**, 2733 (1975); T. Inoue and T. Maskawa, Prog. Theor. Phys. **54**, 1833 (1975).
- [7] V. Vento, M. Rho and G.E. Brown, Nucl. Phys. **A345**, 413 (1980).
- [8] S. Th  berge, A.W. Thomas, and G.A. Miller, Phys. Rev. D **22**, 2838 (1980); **23**, 2106(E) (1981); A.W. Thomas, S. Th  berge, and G.A. Miller, *ibid* **24**, 216 (1981).

- [9] Y. Nambu and J. Jona-Lasinio, Phys. Rev. **124**, 246 (1961); Phys. Rev. **122**, 345 (1961).
- [10] A. Le Yaouanc, L. Oliver, O. Pène, and J.-C. Raynal, Phys. Rev. D **29**, 1233 (1984).
- [11] A. Le Yaouanc, L. Oliver, O. Pène, and J.-C. Raynal, Phys. Rev. D **31**, 137 (1985).
- [12] S. Adler and A. Davis, Nucl. Phys. B **244**, 469 (1984).
- [13] P. J. Bicudo and J. E. Ribeiro, Phys. Rev. D **42** (1990) 1611.
- [14] P. J. Bicudo and J. E. Ribeiro, Phys. Rev. D **42** (1990) 1625; **42** (1990) 1635.
- [15] F. Llanes-Estrada and S. Cotanch, Phys. Rev. Lett. **84**, 1102 (2000).
- [16] H.G. Dosch Phys. Lett. B **190**, 177 (1987); H.G. Dosch and Yu A. Simonov Phys. Lett. B **205**, 339 (1988).
- [17] P. J. Bicudo, Phys. Rev. C **60** (1999) 035209.
- [18] P. Bicudo and J. Ribeiro, Phys. Rev. C **55** (1997) 834 [arXiv:nucl-th/9703027].
- [19] P. Bicudo, G. Krein and J. Ribeiro, Phys. Rev. C **64**, 025202 (2001).
- [20] P. Bicudo, J. Ribeiro and J. Rodrigues Phys. Rev. C **52**, 2144 (1995).
- [21] P. Bicudo, L.Ferreira, C. Placido and J. Ribeiro, Phys. Rev. C **56**, 670 (1997).
- [22] J. E. Ribeiro, Z. Phys. C **5** (1980) 27.
- [23] S. Lemaire, J. Labarsouque and B. Silvestre-Brac, Nucl. Phys. **A714**, 265, (2003).
- [24] R. Ceuleneer, C. Semay and B. Silvestre-Brac, J. Phys. G **22**, 1395 (1996).
- [25] P. Bicudo, J. E. Ribeiro and A. Nefediev, Phys. Rev. D**65** :085026 (2002).
- [26] J. E. Ribeiro, Phys. Rev. D **25**, 2406 (1982); E. van Beveren, Zeit. Phys. C **17**, 135 (1982).
- [27] J. Dias de Deus and J. Ribeiro Phys. Rev. D **21**, 1251 (1980).
- [28] P. Bicudo, G. Krein, E. Ribeiro and J. Villate, Phys. Rev. D **45**, 1673 (1992).
- [29] V. De Alfaro, S. Fubini, G. Furlan, C. Rosseti, “Currents in Hadron Physics” , Amsterdam, North-Holland, (1973).
- [30] S. L. Adler, Phys. Rev. **137** (1965) B1022.
- [31] H. Garcilazo, P. Sauer, T. Mizutani and M. Pena, Phys. Rev. C **42** 2315 (1990).